Analytica Chimica Acta 1018 (2018) 54–61

Contents lists available at ScienceDirect

Analytica Chimica Acta

journal homepage: www.elsevier.com/locate/aca

Highly-sensitive open-cell LA-ICPMS approaches for the quantification of rare earth elements in natural carbonates at parts-per-billion levels

Chung-Che Wu [a, b, 1], Marcel Burger [b, 1], Detlef Günther [b], Chuan-Chou Shen [a, *], Bodo Hattendorf [b, **]

[a] High-Precision Mass Spectrometry and Environment Change Laboratory (HISPEC), Department of Geosciences, National Taiwan University, 10617 Taipei, Taiwan, ROC
[b] Laboratory of Inorganic Chemistry, Department of Chemistry and Applied Biosciences, ETH Zurich, 8093 Zurich, Switzerland

HIGHLIGHTS

- Development of open-cell LA-ICPMS techniques to measure ultra-trace carbonate REEs using SF-ICPMS with a jet-interface.
- Improvement of detection limits to sub-ng g^{-1} levels.
- Quantification of micro-domain stalagmite REEs containing as low as single digit ng g^{-1}.
- Two recognizable abrupt events with substantial REE anomalies across a 4-mm interval of a stalagmite, deposited during 87-80 ka.

GRAPHICAL ABSTRACT

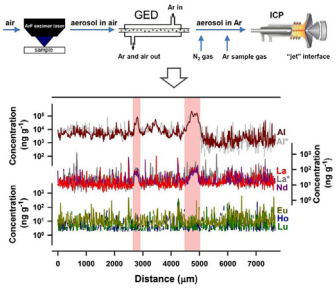

ARTICLE INFO

Article history:
Received 22 August 2017
Received in revised form
2 February 2018
Accepted 4 February 2018
Available online 13 February 2018

Keywords:
Open-cell LA-ICPMS
Carbonates
Rare earth elements
ng g^{-1} techniques

ABSTRACT

This work presents a high-sensitivity approach to quantify ultra-trace concentrations of rare earth elements (REEs) in speleothem carbonates using open-cell laser ablation-sector field-inductively coupled plasma mass spectrometry (open-cell LA-SF-ICPMS). Specifically, open-cell LA in combination with a gas exchange device enabled sampling of large-scale carbonate specimens in an ambient environment. The use of a "jet" vacuum interface and the addition of small amounts of N_2 gas allowed for a 20–40 fold sensitivity enhancement compared to the conventional interface configuration. Mass load effects, quantification capabilities and detection power were investigated in analyses of reference materials using various combinations of spot sizes and laser repetition rates. From a 160 μm diameter circular laser spot and 10 Hz ablation frequency, limits of detection were in the low or sub-ng g^{-1} range for REEs. Little dependence of Ca normalized sensitivity factors on the amount of material introduced into the plasma was observed. Relative deviations of quantified concentrations from USGS MACS-3 preferred values were smaller than 12%. The analytical approach enabled the determination of REE concentration profiles at the single digit ng g^{-1} level. Application to a 15-cm piece stalagmite collected from East Timor revealed at least two abrupt elevations in light rare earth elements (LREEs) within a scanning distance of 8 mm. These anomaly regions extended over a distance of ≈200 μm and showed LREE abundances elevated by at least one order of magnitude. This high-resolution open-cell LA-SF-ICPMS method has the potential to

* Corresponding author. Department of Geosciences, National Taiwan University, No. 1, Sec. 4, Roosevelt Road, 10617 Taipei, Taiwan, ROC.
** Corresponding author. Department of Chemistry and Applied Biosciences, ETH Zurich, Vladimir-Prelog-Weg 1, 8093 Zurich, Switzerland.
E-mail addresses: river@ntu.edu.tw (C.-C. Shen), bodo@inorg.chem.ethz.ch (B. Hattendorf).
[1] These authors contributed equally.

https://doi.org/10.1016/j.aca.2018.02.021

be applied in micro-domain analyses of other natural carbonates, such as travertine, tufa, and flowstones. This is promising for a better understanding of earth and environmental sciences.

1. Introduction

The accurate determination of preserved high-resolution trace-element- and stable-isotope-variations in slowly growing natural carbonates, such as stalagmites, has recently gained extensive attention in the field of geology, earth- and environmental-sciences [1–5]. Stalagmites often grow continuously and can be accurately dated by means of radiometric techniques. Furthermore, they suffer little from secondary alteration and are therefore considered to be ideal multi-proxy archives for past climatic and environmental changes [6–10].

The geochemistry of rare earth elements (REEs) in speleothems, such as stalagmites, has been studied for understanding contemporary and late-quaternary climatic processes [11–13]. Since REEs are enriched in igneous rocks but depleted in carbonates [14], REE series preserved in stalagmites are considered to be an ideal indictor to reconstruct past gigantic volcano eruptions [15].

Diverse analytical methods, including neutron activation analysis (NAA) [16], inductively coupled plasma atomic emission spectrometry (ICPAES) [17], thermal ionization mass spectrometry (TIMS) [18], and inductively coupled plasma mass spectrometry (ICPMS) [19] have been employed for quantitative analyses of REEs in natural carbonates. Specifically, the detection capabilities offered by solution nebulization ICPMS allow multi-element analysis of carbonate REEs at ng g^{-1} to sub-ng g^{-1} levels [19–21]. However, these techniques were all based on discrete mini-domain sampling strategies and time-consuming sample preparation protocols, which prohibited acquisition of high-resolution records (<500 μm) [22] and limited sample throughput. In 2011, Shen et al. [23] developed a fast and precise method, using sector field-inductively coupled plasma mass spectrometry (SF-ICPMS) for the determination of carbonate REEs in femtogram quantities without chemical separation processes. Although a high sample throughput of 8–10 samples per hour could be achieved, steps of physical subsampling, dissolution, and dilution were still required.

Laser ablation sampling in combination with inductively coupled plasma mass spectrometry (LA-ICPMS) offers the capabilities for the rapid, *in-situ* determination of major, minor and trace element concentrations [24,25]. High sensitivity, large linear dynamic range and the possibility to collect data at high lateral resolution between single digit and hundreds of μm make LA-ICPMS a powerful tool for element- and/or isotope-specific microanalyses in solid materials [26].

In conventional LA-ICPMS analyses, the sample of interest needs to be placed inside an enclosing ablation chamber that limits the size of objects that can be analyzed to several centimeters. This constrains the applicability of LA-ICPMS for the analysis of large-scale stalagmites. In 2013, Tabersky et al. [27] introduced an open-cell LA-ICPMS approach that allows analysis of differently sized and shaped samples in an atmospheric environment. Large samples do not need to be cut to fit within an ablation cell anymore, which prevents sample damage and avoids loss of information. Validity of this approach has been tested with various standard reference materials (SRMs). Suitability for the analysis of large-scale stalagmite samples has been demonstrated. REE concentrations in the several hundreds of ng g^{-1} regime could be quantified in glass SRMs using the open-cell LA approach in combination with a quadrupole-inductively coupled plasma mass spectrometer (Q-ICPMS). However, this setup was not sensitive enough to determine REE profiles in the stalagmite sample. This was due to the very low REE abundances in natural carbonates, typically ranging from several hundreds of pg g^{-1} to several tens of ng g^{-1} [11,28].

Here we propose an advanced LA-ICPMS methodology that is based on the combination of open-cell LA with a SF-ICPMS. The use of a jet-interface with the addition of small amounts of N_2 gas allowed a 20–40 fold sensitivity enhancement, which translated into a more than one order of magnitude improvement in limits of detection (LODs). This enabled the quantitative determination of speleothem REE concentrations in the single digit ng g^{-1} range. Emphases were placed on the investigation of mass load effects [29], the evaluation of quantification capabilities, and detection power. Following careful method development, the open-cell LA-SF-ICPMS approach was applied to a stalagmite collected from East Timor. REE concentration profiles showed several possible volcano events within the time period of 79–86 thousand years ago (ka, before 1950 *AD*, hereafter).

2. Analytical procedure

2.1. Instrumentation

All experiments were carried out using a 193 nm ArF excimer LA system (GeoLas C, Lambda Physik, Göttingen, Germany) coupled to a SF-ICPMS (Element XR, Thermo Fisher Scientific, Bremen, Germany). LA was performed on standard reference materials (SRMs) with either a conventional closed ablation chamber, or an open-cell setup. ICPMS detection was carried out operating the Element XR instrument with either standard- or jet-interface configuration.

The closed-cell setup consisted of an air-tightly sealing cylindrical ablation chamber that could hold samples of up to 50 mm diameter and offered a total volume of 63 mm^3 [30]. The open-cell setup comprised an aerosol entrainment device (MANTA) that allowed LA sampling from almost arbitrarily sized objects and a large-capacity gas exchange device (GED, J-SCIENCE Lab Co., Ltd., Kyoto, Japan). By means of a membrane pump, the laser-generated aerosols were extracted from the sampling site and delivered to the GED. Within the GED, the air was exchanged with argon to allow for operation of the ICP [27]. Specifically, with the open-cell setup, LA sampling was just limited by the scanning range of the translation stage (>230 mm in length, 34 mm in width, and 16 mm in height). Fig. 1 provides a schematic representation of the open-cell LA-SF-ICPMS approach. A detailed description and evaluation of this methodology can be found in the literature [27].

In standard configuration, the vacuum interface of the SF-ICPMS comprised a standard sampler cone and a nickel X skimmer cone (X-version, Thermo Fisher Scientific, Waltham, USA). In jet configuration, the standard sampler cone was replaced with a jet sampler cone (JET-version, Thermo Fisher Scientific, Waltham, USA). Additionally, a high capacity vacuum pump was used to maintain the pressure gradient between the ICP, the interface region and the mass analyzer. Small amounts of N_2 gas were admixed to the carrier gas stream before the aerosol was introduced into the ICP torch.

Operating parameters of the LA-SF-ICPMS setup are reported in Table 1. They were adjusted to allow maximum sensitivity for ^{238}U

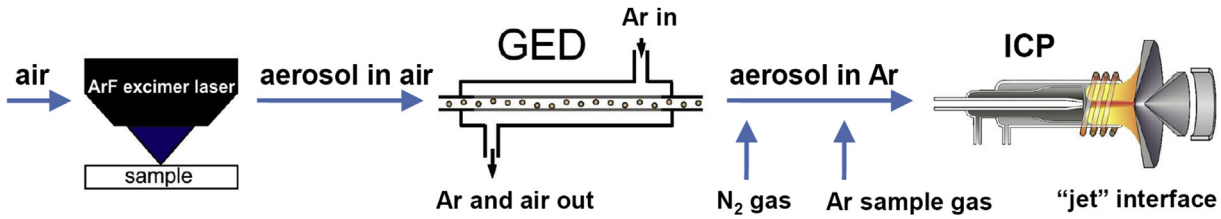

Fig. 1. Schematic representation of the open-cell LA-SF-ICPMS approach. The airborne aerosol is introduced into a GED where the air is exchanged with argon. Upstream of the ICP torch, Ar carrier gas is added. When the jet-interface is used, a minute amount of N_2 gas is supplied as well. Detection is carried out by SF-ICPMS.

Table 1
Operating parameters of the LA-SF-ICPMS setup.

Laser ablation system: GeoLas C	
Wavelength	193 nm
Pulse duration	16 ns
Laser fluence	14–17 J cm^{-2}
Laser spot size	16–160 μm
Laser repetition rate	5–40 Hz
*Carrier gas flow (He)	1.0–1.2 L min^{-1}
#Carrier gas flow (Air)	0.8–0.9 L min^{-1}
#Sweep gas flow (Ar)	8.0–10 L min^{-1}
ICPMS: Element XR	
Sample gas flow (Ar)	0.8–1.0 L min^{-1}
Auxiliary gas flow (Ar)	0.8–1.2 L min^{-1}
Cooling gas flow (Ar)	16 L min^{-1}
RF power	1225–1500 W
N_2 gas flow (jet-interface)	15–20 mL min^{-1}
Mass resolving power ($M/\Delta M$)	Low (300)
Samples per peak	20
Integration time	8 ms
Integration window	40%
Integration type	Average
Time per sweep	0.49 s
Distance per sweep	4.9 μm
Detector mode	Triple
$^{232}Th^{16}O^+/^{232}Th^+$	0.3–0.5%
$^{238}U^+/^{232}Th^+$	0.98–1.02

* applied only to the closed-cell setup.
# applied only to open-cell setup.

while maintaining high sensitivity for a broad mass to charge (m/z) range, low oxide formation rates and similar ^{238}U and ^{232}Th sensitivities. They were determined for every instrumental approach separately from ablation of NIST SRM 612 with a 16 μm diameter circular laser spot, 10 Hz ablation frequency and 10 μm s^{-1} scan speed.

2.2. Experimental design

Sensitivities have been determined for the closed-cell and the open-cell setup. Both setups have been tested with the standard- and the jet-interface. LA was carried out on NIST SRM 612 with a laser spot of 160 μm, 10 Hz ablation frequency and a scan speed of 10 μm s^{-1}.

Mass load effects were investigated by evaluating the abundance corrected sensitivities and the variation of sensitivity ratios to the internal standard as a function of the area ablated with circular laser spots of variable diameters in the range from 16 μm to 160 μm. Given the homogeneous beam profile delivered by the LA system used in this study, the area ablated with a certain spot is considered a direct measure for the mass load introduced into the system.

Quantification capabilities of the open-cell LA-SF-ICPMS approach were tested in analyses of NIST SRM 612, NIST SRM 614 and USGS MACS-3. Relative sensitivity factors were determined from ablation of NIST SRM 610 (analysis of NIST SRM 612 and NIST SRM 614) and NIST SRM 614 (analysis of USGS MACS-3).

2.3. Data collection, processing, and evaluation

Data was acquired following a standard sample standard bracketing protocol comprising data from acquisitions of an external reference material to establish relative sensitivities, unknown samples, and an external reference material again to correct for instrument drift. This sequence is a conventional protocol for ICPMS analyses such as Q-ICMPS [15,27] or time-of-flight ICPMS (TOF-ICPMS) [31,32]. For each individual acquisition, gas blank signal intensities were determined and used as a measure for background signal intensities and subtracted from the signals recorded during ablation.

Quantification was performed using an in-house developed software package STALQUANT [33] that follows the algorithm proposed by Longerich et al. [34]. Two different quantification schemes were used for calculation of high-resolution concentration profiles and determination of bulk element abundances. High-resolution concentration profiles were established by relating the mass scan acquisition time to the LA sampling position. In these experiments, every data point of a given time trace was quantified individually. Unlike that, bulk concentrations were determined from isotope intensities averaged over the ablation period. In all experiments, ^{44}Ca was selected as the internal standard isotope.

The critical level of an analysis has commonly been calculated by taking three times the standard deviation of a gas blank as a measure for the background noise [34]. Here, the instrumental REE background intensities consisted of stochastic single ion counts. Thus, according to the recommendation of the International Union of Pure and Applied Chemistry (IUPAC), LODs were calculated assuming counting statistics [35] as outlined in the supporting information.

2.4. Stalagmite sample

The stalagmite sample MC 4–2 was collected from Lekiraka cave in East Timor (8°47′10.8″S, 126°23′31.1″E). The cave is located in a region surrounded by hundreds of volcanoes, which form a part of the "Pacific Ring of Fire". The stalagmite sample was sliced into slabs of 1 cm thickness and their surfaces were polished. Slab MC 4–2 analyzed in this study is 15 cm in length and 5 cm in diameter. From slab MC 4–2, several drilling subsamples of 50–100 mg each were taken for U-Th dating [36]. U-Th ages indicated that this stalagmite grew in the time period from 101 to 73 ka.

The stalagmite sample MC 4–2 was analyzed using the open-cell LA-SF-ICPMS approach developed in this study. Spatially resolved trace element concentration profiles were calculated from time traces recorded in two individual line scanning experiments. In both studies, the stalagmite was scanned across a distance of 8 mm that covered the time period from 86 to 78 ka. The ablation tracks were running in parallel to each other and were separated by several 100 μm. Both experiments were carried out with a 160 μm

diameter circular laser spot and an ablation frequency of 10 Hz. The scan speed of 10 μm s^{-1} resulted in a lateral displacement of 4.9 μm for an entire mass scan. Prior to the acquisition of high-resolution concentration profiles, the sample surface was cleaned with a low energy LA routine (3.7 J cm^{-2} fluence, 160 μm diameter circular laser spot, 10 Hz ablation frequency, 10 μm s^{-1} scan speed).

The average elemental composition of the anomaly layer and the adjacent baseline regions were investigated with hole drilling experiments. These studies were performed with a 160 μm diameter circular laser spot and 10 Hz ablation frequency.

For line scanning and hole drilling experiments, NIST SRM 614 was used as the calibration standard to establish relative sensitivity factors. Specifically, NIST SRM 614 was selected as external reference material [37–39] because its lower REE levels (720–813 ng g^{-1}) better match the expected speleothem REE concentrations than USGS MACS-3 or the more frequently used NIST SRM 612 or NIST SRM 610 [15,40,41].

Stoichiometry of the stalagmite sample was assumed as pure calcite and a Ca concentration of 400,000 mg kg^{-1} was used for internal standardization. This estimation cannot account for changes in the matrix composition and quantitative results will be biased when carbonate samples with variable concentrations of trace elements, organic material, and/or detritus are analyzed. However, this simplification was considered appropriate for the purpose of this study.

Signal intensities recorded from ablation of the stalagmite sample were occasionally spiking. This observation was attributed to remobilization of large particulates that got previously deposited at the walls of the MANTA, the aerosol transfer lines or the membranes within the GED. These spikes were removed from the time traces in an offline data processing routine. Data points that showed deviations exceeding a threshold of three times the standard deviation of the mean ion signal intensity calculated from its two adjacent data points were excluded from analysis. The average isotopic intensity was calculated as geometric mean, the standard deviation was derived assuming counting statistics.

3. Results and discussion

3.1. Abundance corrected sensitivities as a function of the instrumental setup

Fig. 2 displays abundance corrected sensitivities for selected elements. Specifically, the isotope selection is covering a large proportion of the elemental *m/z* range and includes the complete suite of the REEs.

The use of the jet-interface in combination with the addition of small amounts of N_2 gas allowed a sensitivity enhancement by a factor of 20–40. This effect was observed for both, the closed-cell LA and the open-cell LA setup. For example, we found that the abundance corrected sensitivities for La were increased from 70 to 1300 cps × g × ng^{-1} (closed-cell LA) and from 13 to 460 cps × g × ng^{-1} (open-cell LA), respectively. This observation could be attributed to an improvement in ion extraction efficiency from the ICP and the first expansion stage enabled by the specific design of the jet sampler cone and the increased pumping speed [42,43]. A 2–4 fold lower sensitivity observable with the open-cell LA setup has already been reported in a previous study [27]. This observation is explained with differences in transport efficiencies and material re-deposition related to the utilization of different carrier gases. For both LA setups, REE background signals intensities were maintained at similar values in the range from 0 to 1000 counts per second (cps) (Fig. S1).

3.2. Mass load effects

Fig. 3A shows abundance corrected sensitivities as a function of the area ablated with circular laser spots of various diameters (16, 24, 44, 60, 90, 120, 160 μm). Results are reported for Al, Ca, La, Ho, Lu and U. These elements were specifically selected to represent trace elements, matrix elements, light rare earth elements (LREE), middle rare earth elements (MREE), heavy rare earth elements (HREE) and actinide elements. Fig. 3B displays the same data normalized to Ca.

The abundance corrected sensitivities reported in Fig. 3A did not increase proportionally to the area ablated with laser spots of variable diameters between 16 μm and 160 μm. For example, for a 100 fold increase in laser spot area, we determined an only 35 fold increase in abundance corrected sensitivity for La. The abundance corrected La sensitivities were 13 and 460 cps × g × ng^{-1} from 16 μm to 160 μm laser spots, respectively. Explanations for this observation include a reduced aerosol transport efficiency with increasing mass load. This could be a result of settling losses that became more significant with increasing mass ablation rate. Greater losses most likely occur within the MANTA because changing the laser repetition rate for a fixed spot size did follow a near-linear trend (Fig. S2). The non-linear dependency of abundance corrected sensitivities from laser spot area is thus less likely a consequence of the changes in absolute aerosol density within the carrier gas, but rather related to the wider aerosol plume expansion after ablation with a larger laser spot.

Importantly, the sensitivity ratios of REEs relative to Ca remained nearly unaffected by the mass load introduced into the system (Fig. 3B). Relative standard deviations computed from seven measurements with spot sizes between 16 μm and 160 μm were 1.1%, 1.8% and 1.9% for La/Ca, Ho/Ca and Lu/Ca sensitivity ratios, respectively. These results are in agreement with previously reported findings [29,44,45] and indicate that there was little mass-load induced fractionation between REEs and Ca. However, Ca normalized U sensitivity ratios decreased by about 10% when the laser spot diameter was changed from 16 μm to 60 μm. This behavior is not yet fully understood but is not expected to have a strong influence on quantitative results obtained when mass load matching between

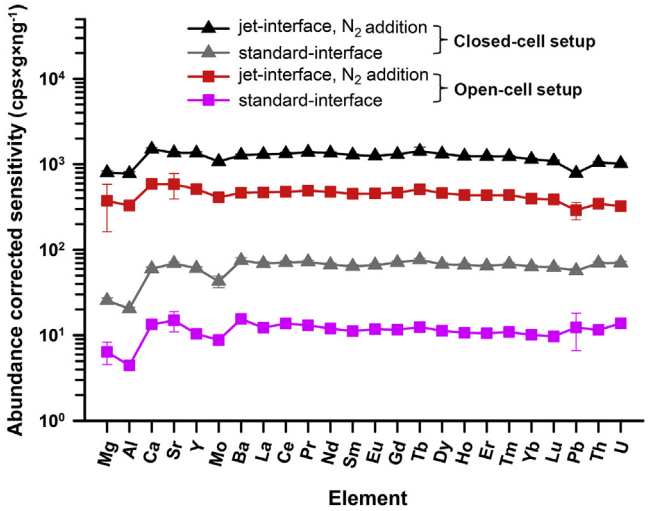

Fig. 2. Abundance corrected sensitivities (cps × g × ng^{-1}) for the selected light-to-heavy elements. Data are reported for the closed-cell and open-cell setup. Both setups have been tested in combination with the jet vacuum interface and the standard vacuum interface. Experiments were carried out on NIST SRM 612 with a 160 μm diameter circular laser spot, 10 Hz ablation frequency and 10 μm s^{-1} scan speed. Error bars indicate the standard deviation of the signal intensity recorded during at least 30 s of ablation.

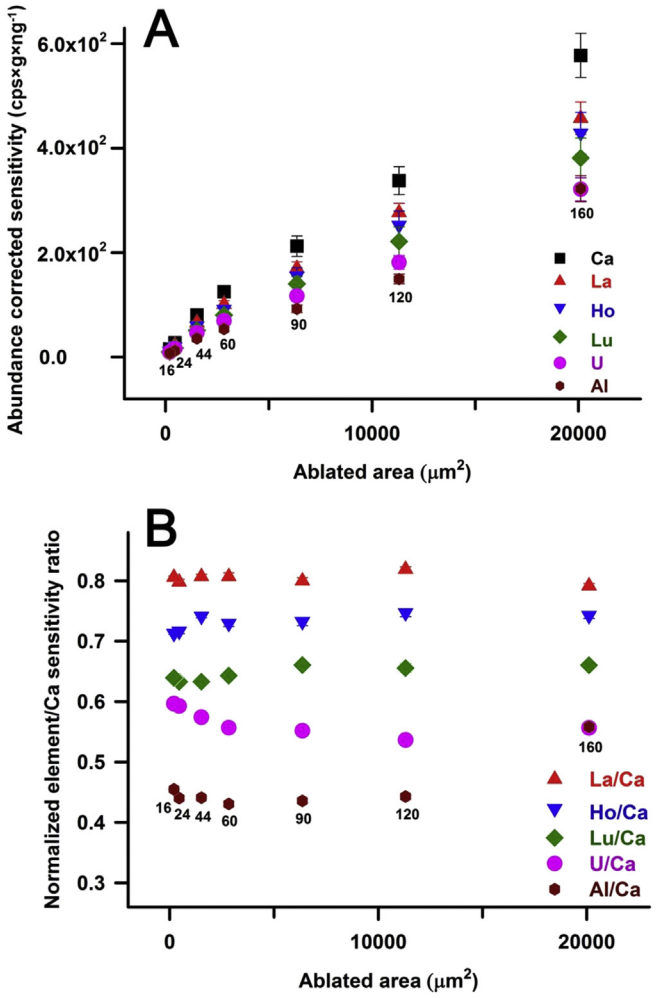

Fig. 3. **(A)** Abundance corrected sensitivities for the selected elements as a function of the area ablated. Experiments have been carried out with the open-cell LA setup coupled to the jet-interface equipped SF-ICPMS. The analyses were carried out with circular laser spots of various diameters in the range from 16 μm to 160 μm, constant ablation frequency of 10 Hz, and a scan speed of 10 μm s^{-1}. LA was performed on NIST SRM 612. The error bars indicate the standard deviation of the signal intensity recorded during at least 30 s of ablation. **(B)** Ca normalized sensitivity ratios calculated from data reported in Fig. 3A.

external reference material and sample is provided. The significant difference in Ca normalized Al sensitivity ratios obtained from ablation with a 120 μm and a 160 μm laser spot is most likely an artifact caused by incorrect cross calibration between the analog mode of the secondary electron multiplier (SEM) which is used to detect Al signal intensity in experiments carried out with laser spots ≤120 μm and the Faraday detector, which was used to register Al signal intensities from 160 μm spots. However, trace element concentrations are orders of magnitude lower in stalagmites than they are in NIST SRM 612. They can be detected using the SEM only and issues related to an incorrect Faraday cross calibration are not expected to affect quantitative REE concentration profiles.

Based on these results, we have decided to use a 160 μm diameter circular laser spot, an ablation frequency of 10 Hz and a scan speed of 10 μm s^{-1} for further experiments.

3.3. Limits of detection as a function of the instrumental setup

Fig. 4 reports LODs calculated using Poisson-based statistics from ablation of NIST SRM 612 and the stalagmite sample MC 4–2 with a 160 μm diameter laser spot using 10 Hz ablation frequency and a scan speed of 10 μm s^{-1}.

For both, the closed-cell LA and the open-cell LA approach, the use of the jet-interface in combination with the addition of small amounts of N_2 gas allowed an improvement of LODs by one to two orders of magnitude. From integration of signal intensities recorded during 30 s of ablation (300 LA pulses) with the open-cell setup, we determined LODs for REEs in the ranges from 0.04 to 0.3 ng g^{-1} and from 0.08 to 0.5 ng g^{-1} for the glass NIST SRM 612 and the stalagmite sample, respectively. However, evaluation of time traces on a single point basis, as required to establish spatially resolved trace element profiles in the stalagmite, would result in approximately 35 times increased LODs. This is a result of the shorter integration period.

In another study, Jochum et al. [45] determined LODs for REEs in speleothems using a 213 nm LA system coupled to the Element 2 SF-ICPMS with the standard-interface configuration. LA was performed in a closed ablation chamber with a 110 μm diameter circular laser spot and 10 Hz ablation frequency. LODs were in the range from 0.5 to 5 ng g^{-1}. These calculations were based on the conventional 3σ approach proposed by Longerich et al. [34]. Following this approach would lower the LOD estimates for the experiments reported in this study by approximately one order of magnitude in cases of low background signal intensities.

SF-ICPMS typically provides high ion transmission and usually low instrumental background, which translates into low LODs. However, magnetic scanning limits the scan speed and therefore the isotope coverage when short transient signals need to be registered. The open-cell LA approach can also interface with other types of ICPMS instruments, such as Q-ICPMS or TOF-ICPMS, while the jet-interface is currently available for the sector field instruments of Thermo Fisher.

3.4. Evaluation of accuracy and precision

Fig. 5 reports recoveries calculated for the analysis of USGS MACS-3. Here, the recovery was defined as the ratio between the quantified concentration for a given element and its reference concentration reported in the GeoReM database [46]. We found recoveries in the range from 0.9 to 1.1 for most of the elements

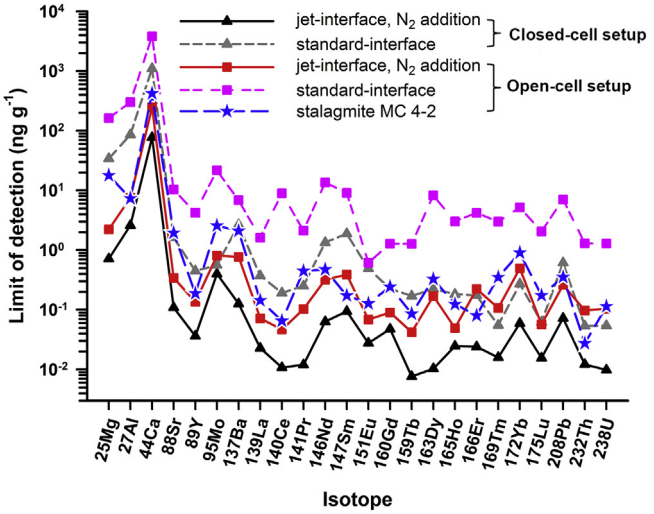

Fig. 4. Limits of detection (LODs) obtained for NIST SRM 612 and the stalagmite sample using a 160 μm diameter circular laser spot, 10 Hz ablation frequency and a scan speed of 10 μm s^{-1}. LODs are based on counting statistics [35].

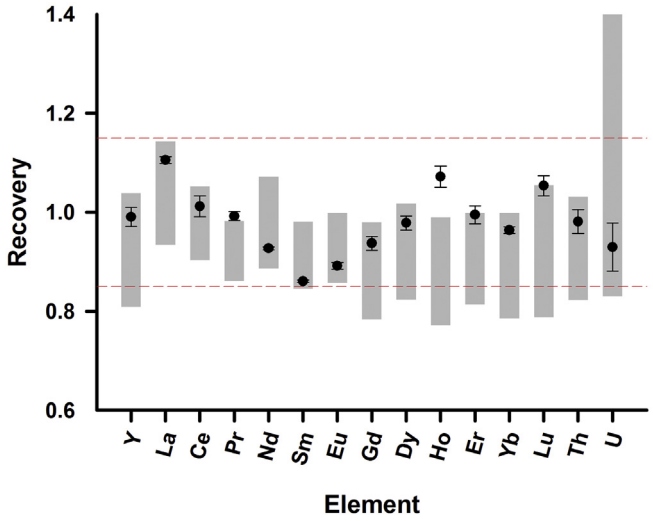

Fig. 5. Recoveries determined for the selected elements in USGS MACS-3. The experiment has been carried out with the open-cell LA setup coupled to the jet-interface equipped SF-ICPMS. LA was performed for at least 30 s with a 160 μm diameter circular laser spot, 10 Hz ablation frequency and 10 μm s^{-1} scan speed. The error bars represent the standard deviation calculated from four replicate measurements. The grey bars indicate the range of concentrations reported on the GeoReM database [46]. The dashed red lines show the ±15% interval of the GeoReM preferred data. (For interpretation of the references to colour in this figure legend, the reader is referred to the Web version of this article.)

studied. Apart from Ho, the quantified REE concentrations agreed with the USGS MACS-3 reference values when the respective uncertainties were taken into account. Quantitative results of the analyses of USGS MACS-3, NIST SRM 612 and NIST SRM 614 are reported in Table S1. Relative deviations from reference concentrations were typically smaller than 12%.

In these experiments, we have studied the internal, as well as the external precision of the open-cell LA-SF-ICPMS approach. Internal precision was defined as the variability of the element concentrations over a single measurement. External precision was defined as the variability of the element concentrations of repeat measurements.

From LA of USGS MACS-3, we determined internal precisions in the range from 0.2 to 1.7% (one standard error of the mean, 1 σ_m). External precision calculated from data of twenty replicate measurements carried out over the course of half a month was in the range from 2.6 to 10% (one relative standard deviation, 1 RSD) (Table S2). As an example, the external uncertainty of the La concentrations in USGS MACS-3 was 3.0%, 2–13 times larger than internal ones (Fig. S3). The higher external uncertainties could be a result of time-dependent instrumental mass discrimination that cannot be fully corrected for or potential heterogeneity of the pressed powder pellet. The high internal precision demonstrated that this open-cell LA-SF-ICPMS approach is suitable to determine high-resolution element concentration profiles by evaluating time traces of signal intensities on a single point basis.

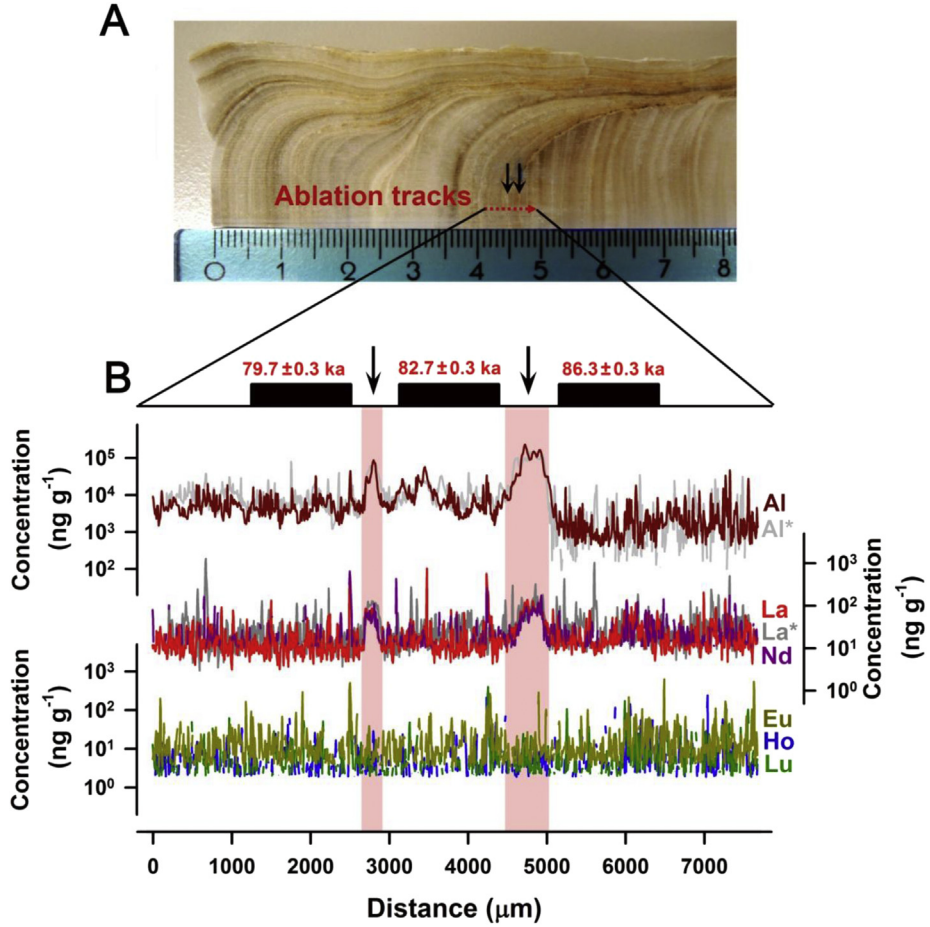

Fig. 6. **(A)** A photograph of an 8 cm segment of the stalagmite sample MC 4–2. The red dotted line indicates the position of the ablation tracks. The two black arrows point at the regions with elevated LREE contents. **(B)** Al and REE concentration profiles obtained by scanning along the red dotted line. Al* and La* profiles have been obtained from a second line scanning ablation paralleling the first one. The black horizontal bars denote locations where subsamples for U-Th dating were taken from. Al and LREE profiles show two pronounced anomalies at distances of 2700–2900 μm and 4500–5000 μm. These intervals correspond to the time periods of 79–82 and 82–86 ka (pink vertical bars). (For interpretation of the references to colour in this figure legend, the reader is referred to the Web version of this article.)

3.5. Microanalytical assessment of a stalagmite sample

Fig. 6 shows concentration profiles for selected elements. The profiles calculated from two individual experiments using the line scanning approach were in good agreement. Distinct anomalies in particular for Al and LREE concentrations were observed within two regions. These intervals were extending from 2700 to 2900 μm and from 4500 to 5000 μm, corresponding to growth periods of 79.7–82.8 and 82.8 to 86.3 ka. These anomaly regions showed Al and LREE concentrations that were enhanced by 2–17 times with respect to their pre- and post-anomaly region baselines. For example, Al concentrations were found to increase from baseline levels between 5.3×10^3 ng g^{-1} (1–2400 μm) and 2.5×10^3 ng g^{-1} (5300–7500 μm) to peak values of 1.3×10^5 ng g^{-1}. La was present at baseline concentrations of 17–18 ng g^{-1} while concentrations of 87 ng g^{-1} were determined within the anomaly regions. Box plots of the Al and La concentrations determined within the different regions of the stalagmite have been calculated (Fig. S4). They further indicate that differences in Al and La concentrations between the anomaly and pre-/post-anomaly regions are significant.

In addition to the line scanning LA experiments that produce spatially resolved concentration profiles, the elemental composition of one anomaly region (≈4800 μm) and the adjacent baseline regions (≈5800 μm and ≈3800 μm) was also analyzed in single hole drilling experiments. For La, we determined a baseline concentration of 12–13 ng g^{-1} while a concentration of 295 ng g^{-1} was determined within the anomaly layer. The differences observed between anomaly region concentrations determined using the line scanning and the single hole drilling approach can be attributed to the different sampling methods and the finite size of the anomaly region. While the single hole drilling approach ideally samples a constant fraction of the anomaly region, the line scanning continuously traverses this region and the aerosol dispersion essentially dilutes material with higher trace element contents. In general, the concentrations of major, minor and trace elements determined in hole drilling experiments are comparable with the ones obtained from line scanning studies (Table S3).

The post-Archean Australian shale (PAAS) [47] normalized REE diagram of the anomaly region (≈4800 μm) has been calculated from data recorded following the single hole drilling protocol. It is characterized by a flat pattern with a positive Eu anomaly. This pattern shows a similar trend as the volcano Toba caldera [48] and andesite rock [13] (Fig. 7). Elevations in Al and LREE concentrations suggest an excess of siliceous rocks and ashes. Volcanic eruptions might be the main contributors to these anomalies.

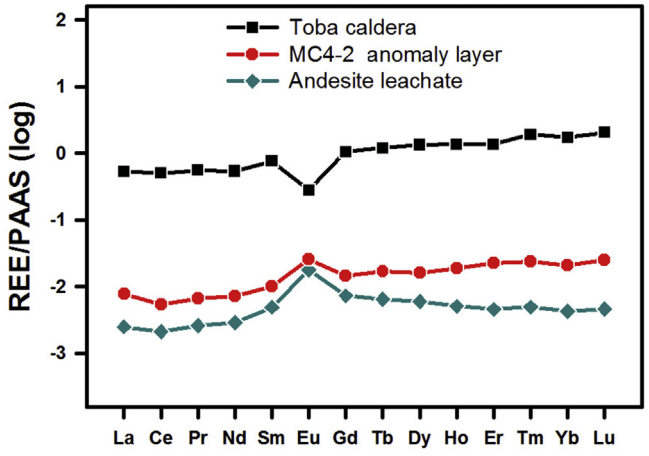

Fig. 7. Comparison of shale-normalized [47] REE patterns of stalagmite MC 4–2, andesite rock and Toba volcano caldera. The normalized REE pattern of the stalagmite MC 4-2 has been calculated from data acquired in a hole drilling experiment. This measurement was carried out within the anomaly region (≈4800 μm in Fig. 6).

4. Conclusions

An open-cell LA setup with a gas exchange device (GED) was coupled to a high sensitivity jet-interface equipped SF-ICPMS. This instrumental approach was characterized with standard reference materials and its suitability for the acquisition of high-resolution trace and ultra-trace element concentration profiles in stalagmites that exceed the dimensions of a conventional ablation cell has been demonstrated.

The use of the jet-interface and addition of small amounts of N_2 gas to the carrier gas achieved a sensitivity enhancement by a factor of 20–40 when compared to the standard interface configuration. From LA with a 160 μm diameter circular laser spot, 10 Hz ablation frequency and 10 μm s^{-1} scan speed, we could obtain LODs in the sub-ng g^{-1} range for REEs. Little differences in mass load effects were observed for Ca and REEs. The standard sample standard bracketing strategy yielded a satisfactory accuracy for trace and ultra-trace element determinations in carbonate and silicate reference materials. Relative deviations from reference concentrations were typically smaller than 12%.

Application of this open-cell LA-SF-ICPMS approach to a stalagmite sample collected from East Timor revealed two abrupt elevations in LREE concentrations within a scanning distance of 8 mm. These anomaly regions extended over a distance of ≈200 μm and showed LREE abundances elevated by at least one order of magnitude with respect to their baseline concentrations. Comparison of the line scanning and the single hole drilling approach indicated that element concentration profiles can readily be obtained in speleothem carbonates. A notable limitation of the scanning approach with the open-cell LA setup was the occurrence of signal spikes, which most likely arose from remobilized particles. Nevertheless, this work highlights the potential and the applicability of our high-sensitivity open-cell LA-ICPMS methodology for paleo-climatic and paleo-environmental studies.

Acknowledgement

This study was supported by an overseas research project provided by Taiwan ROC MOST (104-2917-I-002-007). The analytical methodology was developed at the Laboratory of Inorganic Chemistry, Department of Chemistry and Applied Biosciences, ETH Zurich, founded by SNF grant (Nr. 200021_162870/1). The stalagmite U-Th ages were determined at the High-Precision Mass Spectrometry and Environment Change Laboratory (HISPEC), Department of Geosciences, National Taiwan University, supported by grants from Taiwan ROC MOST (105-2119-M-002-001, 106-2628-M-002-013 to C.-C.S.) and National Taiwan University (105R7625 to C.-C.S.). Authors thank Dr. Ronald A. Harris of the Brigham Young University and Nicole L. Cox of the University of Ballarat for their help in the field. Dr. Henry Longerich is thanked for valuable suggestions and corrections of this manuscript. The three anonymous reviewers helped to improve this manuscript significantly. Their contributions are greatly appreciated.

Appendix A. Supplementary data

Supplementary data related to this article can be found at https://doi.org/10.1016/j.aca.2018.02.021.

References

[1] F.W. Cruz, S.J. Burns, M. Jercinovic, I. Karmann, W.D. Sharp, M. Vuille, Evidence

of rainfall variations in Southern Brazil from trace element ratios (Mg/Ca and Sr/Ca) in a Late Pleistocene stalagmite, Geochem. Cosmochim. Acta 71 (2007) 2250–2263.
[2] D. Fleitmann, S.J. Burns, M. Mudelsee, U. Neff, J. Kramers, A. Mangini, A. Matter, Holocene forcing of the indian monsoon recorded in a stalagmite from southern Oman, Science 300 (2003) 1737–1739.
[3] I.J. Fairchild, P.C. Treble, Trace elements in speleothems as recorders of environmental change, Quat. Sci. Rev. 28 (2009) 449–468.
[4] Y.J. Wang, H. Cheng, R.L. Edwards, Z.S. An, J. Wu, C.-C. Shen, J. Dorale, A high-resolution absolute-dated late pleistocene monsoon record from hulu cave, China, Science 294 (2001) 2345–2348.
[5] P.C. Treble, J.M.G. Shelley, J. Chappell, Comparison of high resolution sub-annual records of trace elements in a modern (1911–1992) speleothem with instrumental climate data from southwest Australia, Earth Planet Sci. Lett. 216 (2003) 141–153.
[6] I.J. Fairchild, A. Baker, A. Borsato, S. Frisia, R.W. Hinton, F. McDermott, A.F. Tooth, Annual to sub-annual resolution of multiple trace-element trends in speleothems, J. Geol. Soc. 158 (2001) 831–841.
[7] W.B. White, Cave sediments and paleoclimate, J. Cave Karst Stud. 69 (2007) 76–93.
[8] P.C. Treble, J. Chappell, J.M.G. Shelley, Complex speleothem growth processes revealed by trace element mapping and scanning electron microscopy of annual layers, Geochem. Cosmochim. Acta 69 (2005) 4855–4863.
[9] F. McDermott, Palaeo-climate reconstruction from stable isotope variations in speleothems: a review, Quat. Sci. Rev. 23 (2004) 901–918.
[10] I.J. Fairchild, C.L. Smith, A. Baker, L. Fuller, C. Spötl, D. Mattey, F. McDermott, Modification and preservation of environmental signals in speleothems, Earth Sci. Rev. 75 (2006) 105–153.
[11] H. Zhou, Q. Wang, J. Zhao, L. Zheng, H. Guan, Y. Feng, A. Greig, Rare earth elements and yttrium in a stalagmite from Central China and potential paleoclimatic implications, Palaeogeogr. Palaeocl 270 (2008) 128–138.
[12] D.K. Richter, T. Götte, S. Niggemann, G. Wurthet, REE3+ and Mn2+ activated cathodoluminescence in lateglacial and Holocene stalagmites of central Europe: evidence for climatic processes? Holocene 14 (2004) 759–767.
[13] M. Hori, T. Ishikawa, K. Nagaishi, C.-F. You, K.-F. Huang, C.-C. Shen, A. Kano, Rare earth elements in a stalagmite from southwestern Japan: a potential proxy for chemical weathering, Geochem. J. 48 (2014) 73–84.
[14] S.R. Taylor, S.M. McLennan, The composition and evolution of the continental crust: rare earth element evidence from sedimentary rocks [and discussion], Phil. Trans. Roy. Soc. Lond. 301 (1981) 381–399.
[15] Z. Siklósy, A. Demény, T.W. Vennemann, S. Pilet, J. Kramers, S. Leél-Össsy, M. Bondár, C.-C. Shen, E. Hegner, Bronze Age volcanic event recorded in stalagmites by combined isotope and trace element studies, Rapid Commun. Mass Spectrom. 23 (2009) 801–808.
[16] M. Scherer, H. Seitz, Rare-earth element distribution in Holocene and Pleistocene corals and their redistribution during diagenesis, Chem. Geol. 28 (1980) 279–289.
[17] I. Kawabe, Y. Kitahara, K. Naito, I. Kawabe, Y. Kitahara, K. Naito, Non-chondritic yttrium/holmium ratio and lanthanide tetrad effect observed in pre-Cenozoic limestones, Geochem. J. 25 (1991) 31–44.
[18] E. Sholkovitz, G.T. Shen, The incorporation of rare earth elements in modern coral, Geochim. Cosmochim. Acta 59 (1995) 2749–2756.
[19] G.E. Webb, B.S. Kamber, Rare earth elements in Holocene reefal microbialites: a new shallow seawater proxy, Geochem. Cosmochim. Acta 64 (2000) 1557–1565.
[20] J. Baker, T. Waight, D. Ulfbeck, Rapid and highly reproducible analysis of rare earth elements by multiple collector inductively coupled plasma mass spectrometry, Geochem. Cosmochim. Acta 66 (2002) 3635–3646.
[21] T. Akagi, Y. Hashimoto, F.-F. Fu, H. Tsuno, H. Tao, Y. Nakano, Variation of the distribution coefficients of rare earth elements in modern coral-lattices: species and site dependencies, Geochem. Cosmochim. Acta 68 (2004) 2265–2273.
[22] L.C. Tan, C.C. Shen, Y.J. Cai, L. Lo, H. Cheng, Z.S. An, Trace-element variations in an annually layered stalagmite as recorders of climatic changes and anthropogenic pollution in Central China, Quat. Res. (Tokyo) 81 (2014) 181–188.
[23] C.-C. Shen, C.-C. Wu, Y. Liu, J. Yu, C.-C. Chang, D.D. Lam, C.-J. Chou, L. Lo, K.-Y. Wei, Measurements of natural carbonate rare earth elements in femtogram quantities by inductive coupled plasma sector field mass spectrometry, Anal. Chem. 83 (2011) 6842–6848.
[24] D. Günther, B. Hattendorf, Solid sample analysis using laser ablation inductively coupled plasma mass spectrometry, Trac. Trends Anal. Chem. 24 (2005) 255–265.
[25] B. Hattendorf, D. Günther, Laser ablation inductively coupled plasma mass spectrometry (LA-ICPMS), in: G. Gauglitz, D.S. Moore (Eds.), Handbook of Spectroscopy, Wiley-VCH Inc., New York, 2014, pp. 647–697.
[26] J. Koch, D. Günther, Review of the state-of-the-art of laser ablation inductively coupled plasma mass spectrometry, Appl. Spectrosc. 65 (2011) 155–162.
[27] D. Tabersky, K. Nishiguchi, K. Utani, M. Ohata, R. Dietiker, M.B. Fricker, I.M.D. Maddalena, J. Koch, D. Günther, Aerosol entrainment and a large-capacity gas exchange device (Q-GED) for laser ablation inductively coupled plasma mass spectrometry in atmospheric pressure air, J. Anal. At. Spectrom 28 (2013) 831–842.
[28] C. Bourdin, E. Douville, D. Genty, Alkaline-earth metal and rare-earth element incorporation control by ionic radius and growth rate on a stalagmite from the Chauvet Cave, Southeastern France, Chem. Geol. 290 (2011) 1–11.
[29] I. Kroslakova, D. Günther, Elemental fractionation in laser ablation-inductively coupled plasma-mass spectrometry: evidence for mass load induced matrix effects in the ICP during ablation of a silicate glass, J Anal At Spectrom 22 (2007) 51–62.
[30] B. Hattendorf, Ion Molecule Reactions for the Suppression of Spectral Interferences in Elemental Analysis by Inductively Coupled Plasma Mass Spectrometry, Diss. No. 14926, ETH Zurich, Zurich, Switzerland, 2002.
[31] O. Borovinskaya, S. Gschwind, B. Hattendorf, M. Tanner, D. Günther, Simultaneous mass quantification of nanoparticles of different composition in a mixture by microdroplet generator-ICPTOFMS, Anal. Chem. 86 (2014) 8142–8148.
[32] M. Burger, A. Gundlach-Graham, S. Allner, G. Schwarz, H.A. Wang, L. Gyr, S. L Burgener, B. Hattendorf, D. Grolimund, D. Günther, High-speed, high-resolution, multielemental LA-ICP-TOFMS imaging: Part II. Critical evaluation of quantitative three-dimensional imaging of major, minor, and trace elements in geological samples, Anal. Chem. 87 (2015) 8259–8267.
[33] M.B. Fricker, Design of Ablation Cells for LA-ICP-MS: from Modeling to High Spatial Resolution Analysis Applications, Diss. No. 20780, ETH Zurich, Zurich, Switzerland, 2012.
[34] H.P. Longerich, S.E. Jackson, D. Günther, Laser ablation inductively coupled plasma mass spectrometric transient signal data acquisition and analyte concentration calculation, Anal. At. Spectrom 11 (1996) 899–904.
[35] L.A. Currie, Limits for Qualitative Detection and quantitative determination application to radiochemistry, Anal. Chem. 40 (1968) 586–593.
[36] C.-C. Shen, C.-C. Wu, H. Cheng, R.L. Edwards, Y.-T. Hsieh, S. Gallet, C.-C. Chang, T.-Y. Li, D.D. Lam, A. Kano, M. Hori, C. Spötl, High-precision and high-resolution carbonate 230 Th dating by MC-ICP-MS with SEM protocols, Geochem. Cosmochim. Acta 99 (2012) 71–86.
[37] S.J. Fallon, J.C. White, M.T. McCulloch, *Porites* corals as recorders of mining and environmental impacts: misima Island, Papua New Guinea, Geochem. Cosmochim. Acta 66 (2002) 45–62.
[38] T. Wyndham, M. McCulloch, S. Fallon, C. Alibert, High-resolution coral records of rare earth elements in coastal seawater: biogeochemical cycling and a new environmental proxy, Geochem. Cosmochim. Acta 68 (2004) 2067–2080.
[39] R. Mertz-Kraus, T.C. Brachert, K.P. Jochum, M. Reuter, B. Stoll, LA-ICP-MS analyses on coral growth increments reveal heavy winter rain in the Eastern Mediterranean at 9 Ma, Paleogeogr. Paleoclimatol. Paleoecol 273 (2009) 25–40.
[40] A.G. Grottoli, K.A. Matthews, J. E Palardy, W.F. McDonough, High resolution coral Cd measurements using LA-ICP-MS and ID-ICP-MS: calibration and interpretation, Chem. Geol. 356 (2013) 151–159.
[41] K. Tanaka, T. Yoshio, S. Hiroshi, Determination of rare earth element in carbonate using laser-ablation inductively-coupled plasma mass spectrometry: an examination of the influence of the matrix on laser-ablation inductively-coupled plasma mass spectrometry analysis, Anal. Chim. Acta 583 (2007) 303–309.
[42] Z.C. Hu, Y.S. Liu, S. Gao, W.G. Liu, W. Zhang, X.R. Tong, L. Lin, K.Q. Zong, M. Li, H.H. Chen, L. Zhou, L. Yang, Improved in situ Hf isotope ratio analysis of zircon using newly designed X skimmer cone and jet sample cone in combination with the addition of nitrogen by laser ablation multiple collector ICP-MS, J. Anal. At. Spectrom 27 (2012) 1391–1399.
[43] N. Kivel, H.D. Potthast, I. Günther-Leopold, F. Vanhaecke, D. Günther, Modeling of the plasma extraction efficiency of an inductively coupled plasma-mass spectrometer interface using the direct simulation Monte Carlo method, Spectroc. Acta Pt. B-Atom, Spectrum 93 (2014) 34–40.
[44] B.J. Fryer, S.E. Jackson, H.P. Longerich, The design, operation and role of the laser-ablation microprobe coupled with an inductively coupled plasma mass spectrometer (LAM-ICP-MS) in the earth sciences, Can. Mineral. 33 (1995) 303–312.
[45] K.P. Jochum, D. Scholz, B. Stoll, U. Weis, S.A. Wilson, Q. Yang, A. Schwalb, N. Börner, D.E. Jacob, M.O. Andreae, Accurate trace element analysis of speleothems and biogenic calcium carbonates by LA-ICP-MS, Chem. Geol. 318 (2012) 31–44.
[46] K.P. Jochum, U. Nohl, K. Herwig, E. Lammel, B. Stoll, A.W. Hofmann, GeoReM: a new geochemical database for reference materials and isotopic standards, Geostand. Geoanal. Res. 29 (2005) 333–338.
[47] S.M. McLennan, Rare earth elements in sedimentary rocks; influence of provenance and sedimentary processes, Rev. Mineral. Geochem. 21 (1989) 169–200.
[48] J.A. Westgate, P.A. Shane, N.J. Pearce, W.T. Perkins, R. Korisettar, C.A. Chesner, M.A. Williams, S.K. Acharyya, All Toba tephra occurrences across Peninsular India belong to the 75,000 yr B.P. eruption, Quat. Res. 50 (1998), 107e112.